

Nanostructured metal oxide/conjugated polymer hybrid solar cells by low temperature solution processes

Yun-Yue Lin,^a Chun-Wei Chen,^{*a} Tsung-Hung Chu,^a Wei-Fang Su,^{*a} Chih-Cheng Lin,^{ab} Chen-Hao Ku,^b Jih-Jen Wu^b and Cheng-Hsuan Chen^c

Received 9th July 2007, Accepted 22nd August 2007

First published as an Advance Article on the web 7th September 2007

DOI: 10.1039/b710400f

In this article, we have proposed a nanostructured photovoltaic device based on the ZnO nanostructures/poly(3-hexylthiophene)(P3HT):TiO₂ nanorod hybrid by solution processes at low temperature. An array of ZnO nanorods with a larger size of ~50 nm in diameter and ~180 nm in length are grown to provide direct pathways for efficient charge collection. TiO₂ nanorods with a size of ~5 nm in diameter and ~20–30 nm in length are incorporated into polymers to facilitate charge separation and transport by providing an increased interfacial area and a more effective transport pathway. The device performance with the inclusion of TiO₂ nanorods exhibits a seven times increase in the short circuit current with respect to that without TiO₂ nanorods. The device performance can be further enhanced after completely removing the residual surfactant on the TiO₂ nanorods using the ligand exchange method, giving a short circuit current density of 2.67 mA cm⁻² and a power conversion efficiency of 0.59% under Air Mass 1.5 (100 mW cm⁻²) illumination.

Introduction

Recently, dye-sensitized solar cells based on nanoporous TiO₂ thin films can reach an efficiency as high as 10%.¹ However, the requirement of using liquid electrolytes in dye-sensitized solar cells is still a very challenging issue to be resolved for commercial applications. Considerable research has been focused on developing solid state dye-sensitized solar cells or alternatively, polymer solar cells. Polymer solar cells have attracted a great deal of interest recently due to their potential application in developing low-cost, large-area, mechanically flexible photovoltaic devices.^{2,3} A basic requirement for a photovoltaic material is to generate free charge carriers produced by photoexcitation. Subsequently, these carriers are transported through the device to the electrodes without recombining with oppositely charged carriers. Due to the low dielectric constant of organic materials, the dominant photo-generated species in most conjugated polymers is a neutral bound electron-hole pair (exciton). These neutral excitons can be dissociated from Coulomb attraction by offering an energetically favorable pathway for the electron from the polymer (donor) to transfer onto an electron-accepting species (acceptor). Because the diffusion length of excitons in a semiconducting polymer is usually shorter than 20 nm,⁴⁻⁶ the electron acceptor must be intermixed with polymer at a nanometre length scale to achieve efficient charge separation. The most commonly used structure is the polymer-based bulk heterojunction (BHJ) solar cell, which consists of an electron-accepting network formed randomly within the

polymer matrix. The most popular electron acceptors in BHJ polymer photovoltaic devices are C₆₀ derivatives^{7,8} and nanocrystals such as CdSe^{2,9} or TiO₂¹⁰⁻¹² or ZnO.¹³ After charge separation, electrons and holes must be transported to the opposite electrode before back recombination occurs. Carrier transport in the BHJ photovoltaic devices is usually limited by the poorly formed electron conducting pathway through hopping. A promising photovoltaic device structure consisting of a direct and ordered path for photogenerated electrons to the collecting electrode has been proposed. This can be done by using templated porous nanostructures,¹⁴⁻¹⁷ or vertically oriented nanorods.¹⁸⁻²⁰ A maximum external quantum efficiency of ~10% has been achieved by filling polymer into well-controlled TiO₂ nanopores synthesized using block copolymers as the structure directing agent.¹⁴ However, the infiltration of polymer into the small TiO₂ nanopores is still not a trivial task. Recently, ZnO nanorods grown perpendicularly to the substrate have attracted a great interest since they can be synthesized through simple processes from solution at low temperature. Photovoltaic devices based on conjugated polymer deposited onto ZnO nanorods¹⁹ or nanofibers²⁰ have been demonstrated recently. Although the optimized structural dimension of less than 20 nm between nanorods is desirable, it is still very challenging to control the precise spacing between ZnO nanorods for infiltrating polymer. In ref. 19, an amphiphilic molecular dye interface between ZnO nanorods and the polymer is therefore required to assist charge separation due to the large film pore sizes (~100 nm) between nanorods. In this article, we propose a nanostructured photovoltaic device based on the ZnO/P3HT:TiO₂ hybrid material as shown in Fig. 1 schematically. Thicker ZnO nanorod arrays are grown on the electrode surface to provide a direct pathway for efficient electron collection. The thinner TiO₂ nanorods are then incorporated into polymer to provide larger interfacial areas and more effective conduction

^aDepartment of Materials Science and Engineering, National Taiwan University 106, Taiwan. E-mail: chunwei@ntu.edu.tw; suwff@ntu.edu.tw

^bDepartment of Chemical Engineering, National Cheng Kung University, Tainan, 701, Taiwan

^cCenter for Condensed Matter Sciences, National Taiwan University, Taipei 106, Taiwan

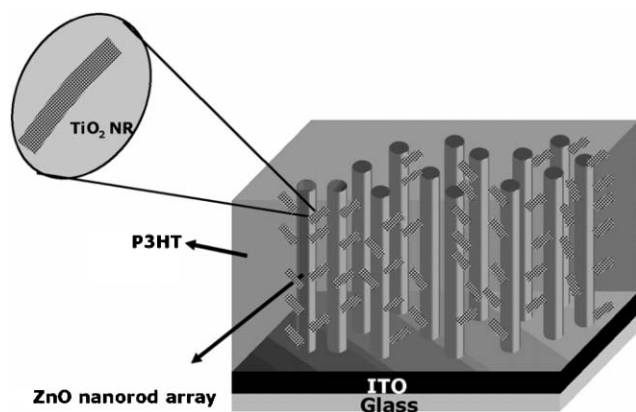


Fig. 1 Schematic representation of the 3D nanostructured photovoltaic device based on the ZnO/P3HT:TiO₂ hybrid material.

paths for charge separation and transport respectively. The mechanisms of efficient charge separation and transport in ZnO/P3HT:TiO₂ nanostructured photovoltaic devices have further been investigated by time-resolved photoluminescence (TRPL) spectroscopy and fast transient photocurrent measurements. Considerable improvement in the device performance can be achieved in the nanostructured hybrid photovoltaic device by infiltrating the P3HT:TiO₂ hybrid material with respect to that obtained by infiltrating the polymer only.

Material preparation and experimental setup

(1) TiO₂ nanorods

The growth of high aspect ratio anatase titanium dioxide nanorods was achieved by the hydrolysis of titanium tetraisopropoxide according to literature methods.^{21,22} Typically, oleic acid (120 g, Aldrich, 90%) was stirred vigorously at 120 °C for 1 h in a three-neck flask under Ar flow, then allowed to cool to 90 °C and maintained at this temperature. Titanium isopropoxide (17 mmole, Aldrich, 99.999%) was then added to the flask. After stirring for 5 min, trimethylamine-*N*-oxide dihydrate (34 mmole, ACROS, 98%) in 17 ml water was rapidly injected. The trimethylamine-*N*-oxide dihydrate was used as a catalyst for polycondensation. The reaction was continued for 10 h to have complete hydrolysis and crystallization. Finally, the TiO₂ nanorods were collected by centrifugation and then redispersed in chloroform. Fig. 2(a) shows the X-ray diffraction (XRD) pattern of TiO₂ nanorods [Philips PW3040 with filtered Cu K α radiation ($\lambda = 1.541 \text{ \AA}$)], indicating the formation of the anatase phase. A sharp peak intensity and narrow width of (004) imply the formation of nanorods. The TiO₂ nanorod microstructure was measured by a JEOL-2000FX (Japan) transmission electron microscope (TEM) operated at 200 keV. The TEM image of TiO₂ nanorods in the inset of Fig. 2(a) reveals that the dimensions of the TiO₂ nanorods are 20–30 nm in length and 4–5 nm in diameter. The high-resolution TEM (HRTEM) image of the TiO₂ nanorods is shown in Fig. 2(b). The corresponding selected-area diffraction pattern (SADP) of the TiO₂ nanorods is also shown in the inset of Fig. 2(b). The *d*-spacing of this ring pattern is 3.54 \AA , 2.39 \AA , 1.90 \AA and 1.69 \AA from inner ring to outer ring. It can

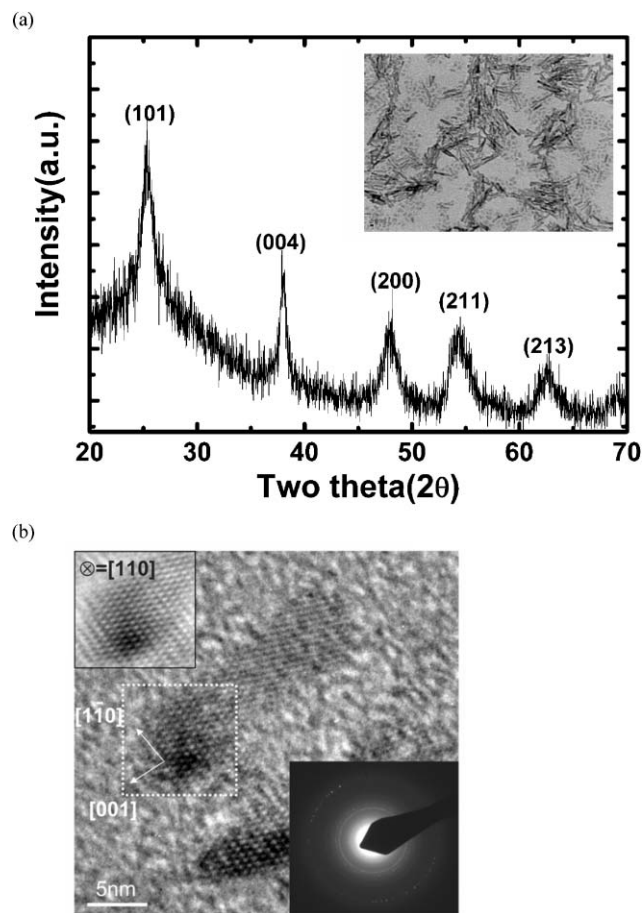


Fig. 2 (a) X-Ray diffraction (XRD) pattern of TiO₂ nanorods. The inset shows the TEM image of TiO₂ nanorods. (b) High-resolution TEM (HRTEM) image of TiO₂ nanorods and the corresponding selected-area diffraction pattern (inset).

be indexed for (101), (004), (200) and (211) of the TiO₂ anatase phase, consistent with the XRD result. The filtered image from the square region is also shown, which indicates the growth direction of the TiO₂ nanorods is along the longitudinal [001] direction in the synthesized condition. In the preparation of hybrid materials, the P3HT solution was prepared by dissolving P3HT (Aldrich, USA) in chloroform at a concentration of 1 wt%. The hybrid materials were prepared by adding the appropriate amount of TiO₂ nanorods to a 1 wt% polymer solution to make composite samples with a ratio of 1 : 1.

(2) Preparation of ZnO nanorods

ZnO nanorod arrays were grown on Au-coated ITO substrates using a pulsed current electrolysis method. Au layers with a thickness of $\sim 10 \text{ nm}$ were pre-deposited on the ITO substrates using DC sputtering. The substrate, a platinum wire and an Ag/AgCl electrode were utilized as the working, the counter and the reference electrodes, respectively, in an electrochemical system. A 0.0025 M aqueous solution of Zn(NO₃)₂ was employed to be the electrolyte. A pulsed wave with a pulse length and a pulse period of 0.01 and 0.1 s, respectively, were used for the growth of ZnO nanorods. The pulsed current density was -2 mA cm^{-2} . Fig. 3(a) shows the typical scanning

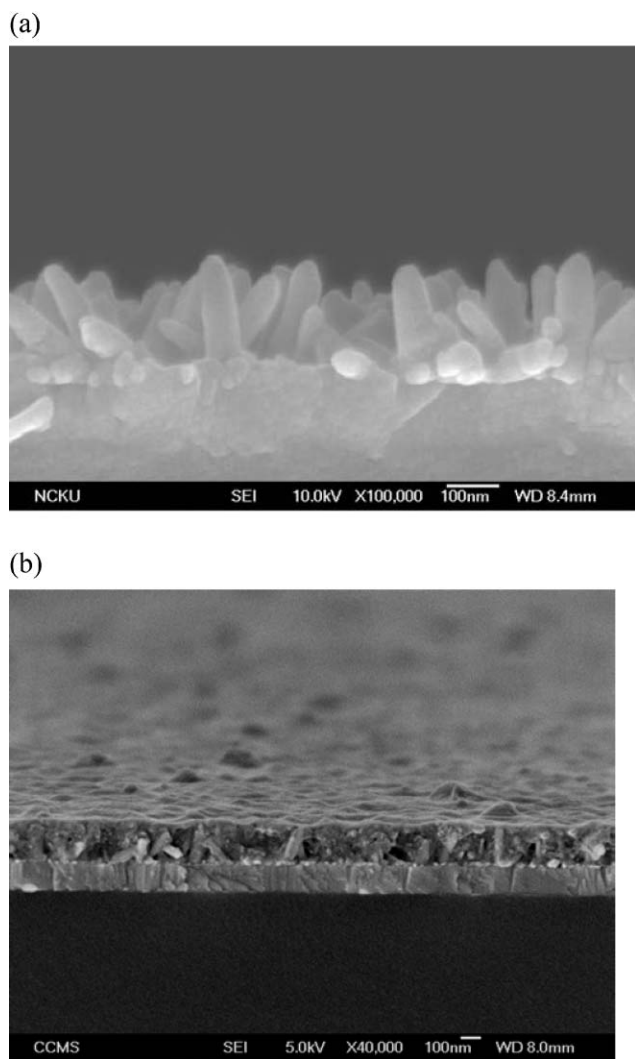


Fig. 3 Cross-sectional SEMs of (a) ZnO nanorod arrays, (b) ZnO nanorods after the infiltration of P3HT:TiO₂ nanorod hybrid.

electron micrograph (SEM) of the ZnO nanorod array formed using a pulsed current electrolysis method at 80 °C. The diameter and the length of the ZnO nanorods are about ~50 nm and ~180 nm, respectively. The average spacing between nanorods is of the order of ~120 nm (estimated from the top view image).

(3) Device fabrication

For photovoltaic device fabrication, a thin active layer consisting of the P3HT:TiO₂ nanorod hybrid was deposited onto ZnO nanorods using spin-coating. The sample was then heated at a temperature of 150 °C for 15 min to facilitate the infiltration of the P3HT:TiO₂ nanorod hybrid. Fig. 3(b) shows the cross-sectional SEM image of the ZnO nanorods after infiltration of the P3HT:TiO₂ nanorod hybrid. The thin active layer with a thickness of 200 nm was used as a light absorbing and hole transporting material. The device was then fabricated by spin-coating a layer of PEDOT:PSS with an effective thickness of 50 nm before thermal evaporation of the Au top electrode. The highly conductive PEDOT:PSS layer is

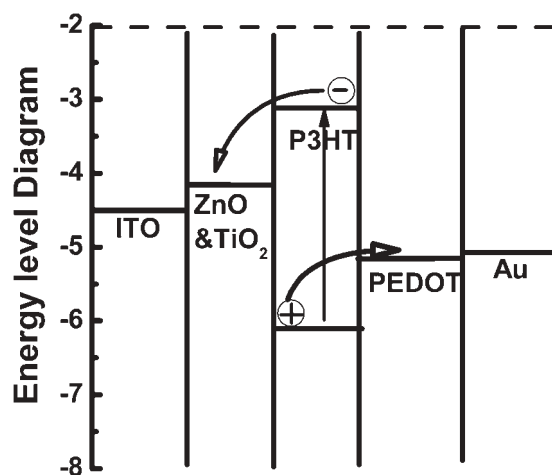


Fig. 4 The corresponding energy levels of the nanostructured photovoltaic device based on ZnO/P3HT:TiO₂ nanorod hybrid.

intended to keep the serial resistance low and to reduce surface roughness by filling the voids in the films. The films were then baked in a vacuum oven for 6 h at 120 °C. Vapor deposition of the Au top electrode was then carried out at pressure around 2×10^{-6} Torr. The corresponding energy levels obtained from the literature^{1,19} for the nanostructured photovoltaic device based on ZnO/P3HT:TiO₂ nanorod hybrid are shown in Fig. 4.

(4) Characterization

UV-Visible absorption spectra were obtained using an Ocean Optics HR-4000 spectrometer. The steady state PL spectra were taken by the FluoroLog®-3 spectrofluorometer (Jobin-Yvon). Time-resolved photoluminescence spectroscopy was performed with a time-correlated single photon counting (TCSPC) spectrometer (Picoquant, Inc.). A pulse laser (375 nm) with an average power of 1 mW operating at 40 MHz with a duration of 70 ps was used for excitation. Current-voltage measurements were obtained using a solar simulator (Oriel Inc.) using the AM 1.5 filter with an irradiation intensity of 100 mW cm⁻². Fast transient photocurrent measurements²³ were performed by a frequency-tripled Nd:YAG pulsed laser ($\lambda = 355$ nm and pulse width ~5 ns) and the signals were recorded by a digital oscilloscope (Tetronix TDS5052B). The film thickness was measured by means of the Veeco M6 surface profiler.

Results and discussions

Fig. 5 shows the normalized absorption spectra of pristine P3HT and ZnO/P3HT:TiO₂ nanorod hybrid thin films respectively. The pristine P3HT exhibits a broad absorption spectrum ranging from 350 to 650 nm. The enhanced optical density of the absorption spectra below 380 nm in the hybrid mainly results from the contributions of ZnO nanorods and TiO₂ nanorods. A slight blueshift of the P3HT band as well as the appearance of a weaker vibronic structure in the hybrid film is mainly attributed to a loss of P3HT polymer-chain stacking after infiltration into ZnO nanorods and mixing with TiO₂ nanorods. As shown in Fig. 4, when the polymer is

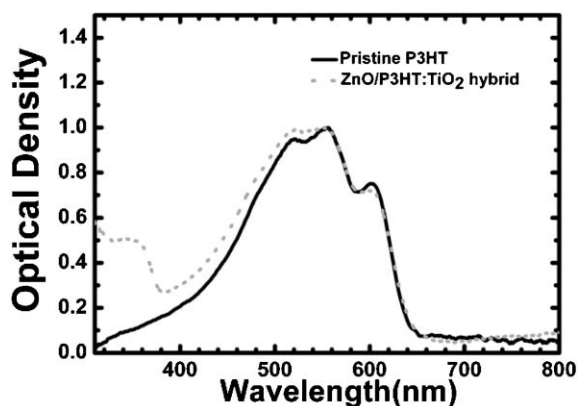


Fig. 5 Normalized absorption spectra of pristine P3HT and ZnO/P3HT:TiO₂ nanorod hybrid thin films respectively.

excited, charge separation occurs at the interface between the polymer and the ZnO (or TiO₂) nanorods, giving a charge-separated state with an electron on the ZnO (or TiO₂) nanorods and a hole on the polymer. Charge separation efficiency at polymer-inorganic nanocrystal interfaces can be usually revealed through quenching of the photoluminescence (PL) efficiency and shortening of the measured PL lifetime in the polymer.^{9,24} Four samples consisting of different configurations are taken for investigation. Sample A (P3HT) represents the pristine P3HT thin film deposited on the ITO substrate. Sample B (ZnO/P3HT) and Sample C (ZnO/P3HT:TiO₂) represent the composites by spin-coating neat P3HT and P3HT:TiO₂ nanorod hybrid thin active layers onto the array of ZnO nanorods respectively. Sample D (ZnO/TiO₂/P3HT:TiO₂) has a similar configuration to Sample C but is pre-coated with a very thin TiO₂ nanorod layer onto ZnO nanorods before the P3HT:TiO₂ nanorod hybrid layer is deposited. The solution concentration of the pre-coated thin TiO₂ nanorods layer is about 10 mg ml⁻¹. After spin-coating the thin TiO₂ nanorod layer, the sample is heat treated at a temperature of 120 °C for 5 min to remove the residual solvent. All these samples have a similar thickness of about 200 nm. Fig. 6 shows the PL decay spectroscopy for the four different samples. It is found that the PL lifetime τ_B (643 ps) for Sample B is shorter than that of the pristine P3HT thin film τ_A (735 ps), indicating that charge separation occurs at the interfaces between P3HT and the ZnO nanorods by providing a new non-radiative process for photogenerated excitons. As TiO₂ nanorods are blended with P3HT, a large number of interfaces between the polymer and the TiO₂ nanorods are generated, leading to more efficient charge separation as a result of the shorter PL lifetime τ_C (509 ps) for Sample C compared to τ_B . For Sample D, the PL decay lifetime τ_D (361 ps) is even shorter than τ_C due to the increasing number of interfaces on the surface of the ZnO nanorods by coating a thin TiO₂ nanorod layer before infiltrating the active layer. As a result, more efficient exciton dissociation occurs. The role of the thin TiO₂ nanorod layer on the ZnO surface can be as follows. Firstly, inserting this layer can create a second interfacial area for exciton dissociation that might increase the charge transfer rate. In addition, an additional TiO₂ nanorod thin film on the ZnO surface can also act as a hole-blocking layer to prevent

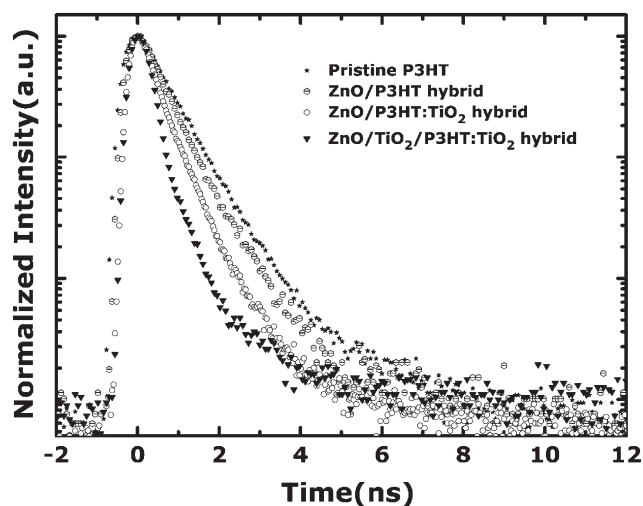


Fig. 6 Time-resolved photoluminescence spectroscopy for the samples consisting of pristine P3HT (Sample A), ZnO nanorods/P3HT (Sample B), ZnO nanorods/P3HT:TiO₂ nanorod hybrid (Sample C) and ZnO nanorods/TiO₂ nanorods/P3HT:TiO₂ nanorod hybrid (Sample D) respectively.

back recombination²⁵ and direct contact between the polymer and the ITO electrode.

The photovoltaic performances of the nanostructured devices based on the ZnO nanorods and P3HT:TiO₂ nanorod hybrid are then characterized under simulated AM 1.5 illumination as shown in Fig. 7. Three devices with different configurations are fabricated for comparison. Device I (ZnO/P3HT) is based on neat P3HT film deposited onto ZnO nanorods and exhibits a short circuit current density (J_{sc}) of 0.30 mA cm⁻², an open circuit voltage (V_{oc}) of 335 mV, a fill factor (FF) of 0.40, and a power conversion efficiency (η) of 0.04%. The η of the device with a neat P3HT film deposited onto ZnO nanorods is similar to that in ref. 19 but is lower compared to that in ref. 20 with a similar configuration. One possible reason for the higher efficiency in ref. 20 may be due

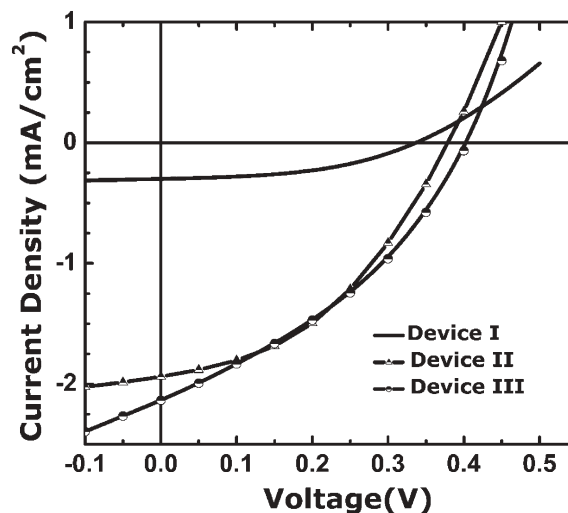


Fig. 7 Photovoltaic performances of devices with different configurations. Device I: (ZnO/P3HT); Device II: (ZnO/P3HT:TiO₂); Device III: (ZnO/TiO₂ nanorods/P3HT:TiO₂).

Table 1 Summary of the device performance of different configurations: Device I: (ZnO/P3HT); Device II: (ZnO/P3HT:TiO₂); Device III: (ZnO/TiO₂ nanorods/P3HT:TiO₂); Device IV: (ZnO/TiO₂ nanorods/P3HT:TiO₂) through pyridine treatment

	$J_{sc}/\text{mA cm}^{-2}$	V_{oc}/mV	FF	η (%)
Device I	0.30	335	0.40	0.04
Device II	1.96	380	0.39	0.29
Device III	2.20	400	0.35	0.31
Device IV	2.67	490	0.45	0.59

to their usage of smaller diameter ZnO nanofibers, which can be infiltrated into more photoactive materials with a higher light harvesting efficiency. Device II has the configuration of ZnO/P3HT:TiO₂ nanorod hybrid and exhibits values for J_{sc} , V_{oc} , FF, and η of 1.96 mA cm⁻², 380 mV, 0.39, and 0.29% respectively. Over six times increase in J_{sc} with respect to Device I is achieved due to increased charge separation and transport efficiency after the inclusion of TiO₂ nanorods in the polymer. Device III has the configuration of ZnO/TiO₂/P3HT:TiO₂ by pre-coating a thin TiO₂ nanorod film onto ZnO nanorods before the infiltration of the P3HT:TiO₂ nanorod hybrid. The device shows J_{sc} , V_{oc} , FF, and η performance of 2.20 mA cm⁻², 400 mV, 0.35, and 0.31% respectively. The further increase in J_{sc} of Device III compared to that in Device II is attributed to the addition of the thin TiO₂ nanorod layer, which prevents electrons from back recombining with holes in P3HT and allows for the photogenerated current to be collected more effectively. Table 1 summarizes the device performance for different configurations. From the photovoltaic performance of the above devices with different configurations, it is found that the inclusion of TiO₂ nanorods in the ZnO/P3HT nanostructured hybrid solar cell can improve the device performance by providing increased interfacial area and a more effective transport pathway. Fig. 8 shows the photovoltaic response decay curves of Devices I and III at the zero bias condition under pulsed laser illumination. A faster responding time ($\sim 0.5 \mu\text{s}$) for the device with the configuration ZnO/TiO₂/P3HT:TiO₂ (Device III) with respect to the device consisting of a neat P3HT film on ZnO nanorods (Device I)

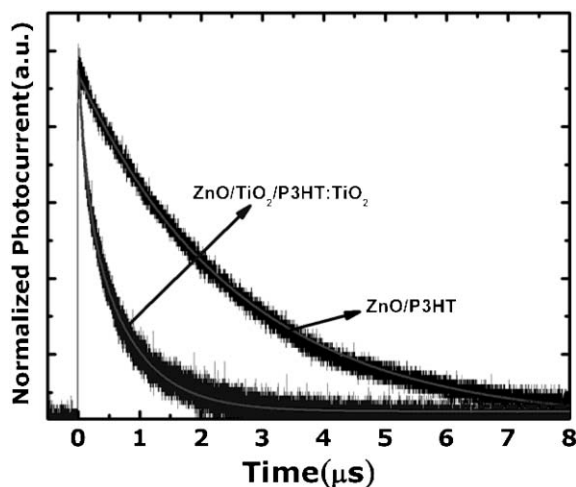


Fig. 8 Fast transient photocurrent decay for Device I (ZnO/P3HT) and Device III (ZnO/TiO₂ nanorods/P3HT:TiO₂) respectively.

($\sim 3.0 \mu\text{s}$) was found, indicating that effective carrier transport can be achieved through this design of hybrid architecture.

In addition, it is suggested that the device performance for the polymer/nanocrystal hybrid solar cells can be further enhanced by completely removing the possible residual surfactant in the hybrid.⁹ We have therefore carried out the process of ligand exchange to remove the residual surfactant oleic acid (OA) through pyridine treatment according to the literature.²⁶ The as-synthesized OA end-capped TiO₂ nanorods were dispersed in pyridine and left stirring at 70 °C until the solution turned clear. Afterwards, the treated nanocrystals were washed with hexane and isolated by centrifugation, and redispersed in pyridine. Through these procedures, the OA (original surface ligand) was removed and the pyridine of a weak binding ligand was on the surface of TiO₂ nanorods, which can be removed through heating. Following the same device fabrication procedures as above, Device IV has a similar configuration to Device III of ZnO/TiO₂/P3HT:TiO₂ by pyridine treatment and shows a short circuit current density

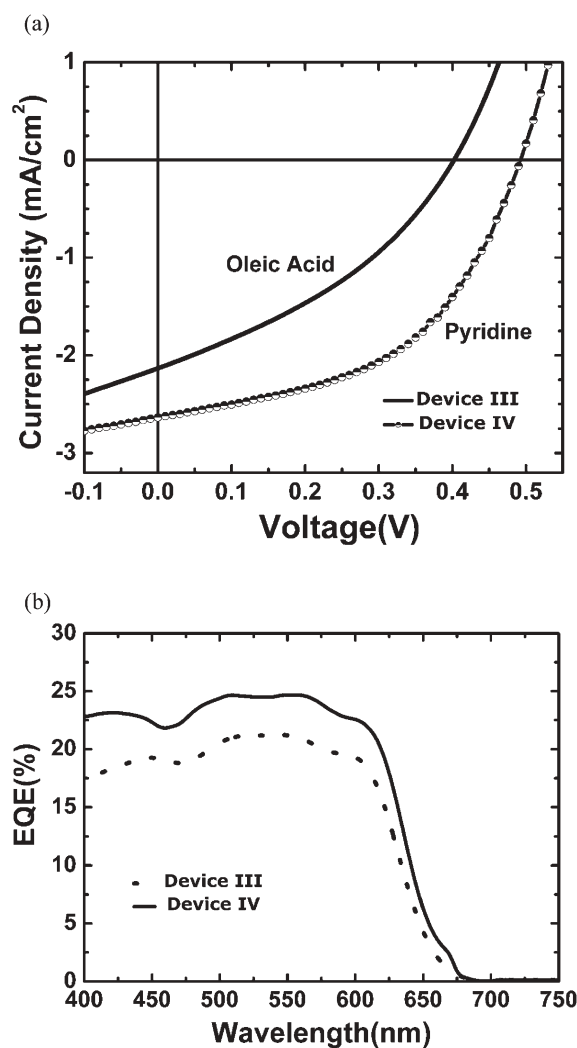


Fig. 9 (a) Photovoltaic performances of the devices before (Device III) and after (Device IV) removing the surfactant (OA) on the TiO₂ nanorods by pyridine treatment. Both the devices have the configuration ZnO/TiO₂ nanorods/P3HT:TiO₂ hybrids. (b) The corresponding external quantum efficiencies (EQE) of Device IV.

(J_{sc}) of 2.67 mA cm^{-2} , an open circuit voltage (V_{oc}) of 490 mV, a fill factor (FF) of 0.45, and a power conversion efficiency η of 0.59% as shown in Fig. 9(a), giving an improvement by nearly a factor of two. The corresponding external quantum efficiency (EQE) of Device IV is shown in Fig. 9(b), which has a maximum value of 24% at 510 nm. Complete removal of the residual surfactant at the P3HT/TiO₂ nanorod interfaces leads to direct contact between the polymer and the TiO₂ nanorods by removing the insulating barrier, leading to a further improvement in charge separation and transport efficiencies. In addition, the increase in the open circuit voltage V_{oc} after pyridine treatment may be attributed to the change in interfacial dipoles, leading to a shift in the band offset at the TiO₂-polymer interface.²⁷

Conclusion

In summary, we have proposed a type of nanostructured polymer/inorganic metal oxide hybrid photovoltaic device through low temperature solution processes. Thicker nanostructured ZnO nanorods are grown on the electrode surface to provide direct pathways for efficient charge collection. Thinner TiO₂ nanorods are incorporated into the polymer to facilitate charge separation and transport by providing increased interfacial area and an effective transport pathway. Considerable improvement in the device performance is achieved by infiltrating the P3HT:TiO₂ nanorod hybrid into ZnO nanorod arrays with respect to that without the incorporation of TiO₂ nanorods. The device performance can be further enhanced after completely removing the residual surfactant in the P3HT:TiO₂ nanorod hybrid after pyridine treatment.

Acknowledgements

This work is supported by National Science Council, Taiwan (Project No. NSC95-2120-M-002-004) and the US Airforce project (AOARD 064-044).

References

- 1 M. Graetzel, *Nature*, 2001, **414**, 338.
- 2 W. U. Huynh, J. J. Dittmer and A. P. Alivisatos, *Science*, 2002, **295**, 2425.
- 3 W. Ma, C. Yang, X. Gong, K. Lee and A. J. Heeger, *Adv. Funct. Mater.*, 2005, **15**, 1617.
- 4 R. H. Friend, G. J. Denton, J. J. M. Halls, N. T. Harrison, A. B. Holmes, A. Kohler, A. Lux, S. C. Moratti, K. Pichler, N. Tessler, K. Towns and H. F. Wittmann, *Solid State Commun.*, 1997, **102**, 249.
- 5 T. J. Savenije, J. M. Warman and A. Goossens, *Chem. Phys. Lett.*, 1998, **287**, 148.
- 6 A. C. Arango, L. R. Johnson, V. N. Bliznyuk, Z. Schlesinger, S. A. Carter and H. H. Horhold, *Adv. Mater.*, 2000, **12**, 1689.
- 7 G. Yu and A. J. Heeger, *J. Appl. Phys.*, 2001, **78**, 4510.
- 8 A. Haugeneder, M. Neges, C. Kallinger, W. Spirkl, U. Lemmer and J. Felmann, *Phys. Rev. B*, 1999, **59**, 15346.
- 9 N. C. Greenham, X. Peng and A. P. Alivisatos, *Phys. Rev. B*, 1996, **54**, 17628.
- 10 J. S. Salafsky, *Phys. Rev. B*, 1999, **59**, 10885.
- 11 C. Y. Kwong, W. C. H. Choy, A. B. Djurisic, P. C. Chui, K. W. Cheng and W. K. Chan, *Nanotechnology*, 2004, **15**, 1156.
- 12 T. W. Zeng, Y. Y. Lin, His-Hsing Lo, C. W. Chen, Cheng-Hsuan Chen, Sz-Chian Liou, Hong-Yun Hunag and Wei-Fang Su, *Nanotechnology*, 2006, **15**, 5387.
- 13 W. J. E. Beek, M. M. Wienk and R. A. J. Janssen, *Adv. Mater.*, 2004, **16**, 1009.
- 14 K. M. Coakley and M. D. McGehee, *Appl. Phys. Lett.*, 2003, **83**, 3380.
- 15 K. M. Coakley, Y. X. Liu, M. D. McGehee, K. L. Frindell and G. D. Stucky, *Adv. Funct. Mater.*, 2003, **13**, 301.
- 16 P. Ravirajan, S. A. Haque, J. R. Durrant, D. D. C. Bradley and J. Nelson, *Adv. Funct. Mater.*, 2005, **15**, 609.
- 17 H. Wang, C. C. Oey, A. B. Djurisic, M. H. Xie, Y. H. Leung, K. K. Y. Man, W. K. Chan, A. Pandey, J. M. Nunzi and P. C. Chui, *Appl. Phys. Lett.*, 2005, **87**, 023507.
- 18 Q. Wei, K. Hirota, K. Tajima and K. Hashimoto, *Chem. Mater.*, 2006, **18**, 5080.
- 19 P. Ravirajan, A. M. Peiró, M. K. Nazeeruddin, M. Graetzel, D. D. C. Bradley, J. R. Durrant and J. Nelson, *J. Phys. Chem. B*, 2006, **110**, 7635.
- 20 D. C. Olson, J. Piris, R. T. Collins, S. E. Shaheen and D. S. Ginley, *Thin Solid Films*, 2006, **496**, 26.
- 21 P. D. Cozzoli, A. Kornowski and H. Weller, *J. Am. Chem. Soc.*, 2003, **125**, 14539.
- 22 Y. T. Lin, T. W. Zeng, W. Z. Lai, C. W. Chen, Y. Y. Lin, Y. S. Chang and W. F. Su, *Nanotechnology*, 2006, **17**, 5781.
- 23 D. H. Auston, *IEEE J. Quantum Electron.*, 1983, **19**, 639.
- 24 Y. Y. Lin, C. W. Chen, J. Chang, T. Y. Lin, Y. S. Liu and W. F. Su, *Nanotechnology*, 2006, **17**, 1260.
- 25 M. Law, L. E. Greene, A. Radenovic, T. Kuykendall, J. Liphard and P. Yang, *J. Phys. Chem. B*, 2006, **110**, 22652.
- 26 W. U. Huynh, J. J. Dittmer, W. C. Libby, G. L. Whiting and A. P. Alivisatos, *Adv. Funct. Mater.*, 2003, **13**, 73.
- 27 Y. Liu, S. R. Scully, M. D. McGehee, J. Liu, C. K. Luscombe, J. M. J. Frechet, S. E. Shaheen and D. S. Ginley, *J. Phys. Chem. B*, 2006, **110**, 3257.